minerals

MDPI

Article

Comminution Effects on Mineral Grade Distribution: The Case of an MVT Lead-Zinc Ore Deposit

Gabriele Baldassarre *, Oliviero Baietto and Paola Marini

Department of Environmental, Land and Infrastructure Engineering (DIATI), Politecnico di Torino; Corso Duca degli Abruzzi, 24, 10129, Turin, Italy; E-mails: gabriele_baldassarre@polito.it, oliviero.baietto@polito.it, paola.marini@polito.it.

* Correspondence: gabriele_baldassarre@polito.it; Tel.: +39-011-090-7614 (G.B., O.B., P.M.)

Received: date; Accepted: date; Published: date

Abstract: Every mining operation is followed by a beneficiation process aimed at delivering quality material to the transformation industry. Mainly, in order to obtain valuable minerals from gangue in mineral processing, comminution and grinding of extracted ore are crucial operations for the following separation steps. Comminution is the most energy consuming phase, and the quality of the results is strictly related to the characteristic of the material under treatment. A preliminary study has been performed in order to understand the crushing behavior of a mixed Zn-Pb sulfide ore and the distribution of the two target minerals among the products of the process. Ore samples have been examined and characterized through thin section observation and SEM analyses for the determination of dimensional grain features, while X-ray powder diffraction (XRPD) quantitative analyses have been performed for the definition of the concentrations. The selected crushing circuit comprises lab-scale equipment. For each stage of the process, products below the free-grain size threshold have been collected, and particle size analyses have been carried out. Comminution products have been divided in dimensional classes suitable for flotation separation, and XRPD analyses showed a mineral grade distribution varying with dimension of the products. This important trend should be considered for further investigation related to an efficient separation.

Keywords: comminution; mineral processing; mixed sulfides; sphalerite; galena;

1. Introduction

The mining industry is deeply characterized by essential operations for a proper transformation process of raw materials into final products. Generally, the exploitation activity in a mine is followed by a beneficiation process designed to increase the quality of the valuable minerals naturally present in the excavated material. The very early stage of the transformation is represented by comminution and grinding of extracted ore aimed at obtaining different changes in terms of dimension and shape of the material that will be further treated [1,2,3]. Progressively, separation processes are set up in order to collect and divide target minerals from gangue and waste.

Comminution is a highly energy consuming operation, and it is characterized by very low efficiency [1,4,5,6] and the quality of the final product being strictly related to physical characteristics of the material under treatment [7,8].

The principal objective of comminution is the realization of mineral liberation, that could be not an easy and predictable outcome but is relevant for an efficient configuration and control of the entire process, especially when the ore has to be delivered to a flotation process [9,10, 11,12,13]. Shape, dimension and distribution of free minerals also play a strategic role for the achievement of an effective beneficiation [14,15].

In this study, the crushing behavior of mixed Pb-Zn sulfide ore, mainly containing galena and sphalerite as valuable minerals, has been analyzed. The separation of these two minerals, usually performed by froth flotation, is highly affected by comminution and grinding stages [16,17,18].

The distribution of concentration of target minerals among the different sized products of the crushing process has been the key focus of this work. All the evaluations brought a clearer overview of how different minerals react to the same comminution pathway.

The importance of having a clear comprehension of the redistribution of target minerals in mid-processing products could lead to an efficient separation. Benefits that could be achieved can enhance a reduction in end-process waste, as well as control of water use, reagents and machinery utilization during the beneficiation stage.

2. Materials and Methods

2.1 Sampling

The mixed Pb-Zn sulfide ore samples come from the Val Vedra mine in the Gorno mining district, Lombardy, Northern Italy. The deposit can be geologically defined as Mississippi Valley Type (MVT), as described in detail by other authors [19], characterized by a mixed sulfide mineralization in a carbonate matrix. About 30 kg of material has been collected during the sampling campaign in order to have a representative set to be studied.

2.2 Characterization Methods for Samples and Products

2.2.1 Optical Microscopy

Optical microscopy (OM) was performed on polished thin sections using a *Leica* optical polarized-light microscope equipped with a *DeltaPix* camera and interfaced with *DeltaPix* software for image acquisition and processing. This was carried out using normal and polarized transmitted light on polished thin sections for the determination of the main features of the mineralization and the average grain size of the target minerals.

2.2.2 Scanning Electron Microscopy

Scanning electron microscopy (SEM) analyses have been performed using a *FEI Inspect S* microscope equipped with an EDAX detector and interfaced with *xT Microscope Control* and *GENESIS XM2i* software. The measurement settings were high vacuum mode, 5.00 kV HV and backscattered electron detector (BSED). Analyses have been performed on uncovered 30 μm thin sections obtained from rock samples.

2.2.3 X-Ray Powder Diffraction Analysis (XRPD)

X-ray powder diffraction (XRPD) analysis was performed using a *Rigaku SmartLab SE* diffractometer, with CuKα radiation at 40kV and 30mA, 5–90° 2θ range, 0.01° step width, 1°/min scan speed equipped with a D/teX Ultra 250 (H) and interfaced with the *SmartLab Studio II* software package. Quantitative phase analyses have been performed by the whole-powder-pattern fitting (WPPF) Rietveld method [20-22] as implemented in the software. A pseudo-Voigt peak shape function has been selected. The refined parameters have been phase scale factor, peak shape parameters, lattice parameters, preferred orientation and structure coefficients. The ICCD PDF-4 2020 database [23] has been used for phase recognition and refining.

2.3 Comminution Flowsheet

Physical treatments have been carried out in order to simulate, on a lab-scale, a possible comminution circuit arrangement for this kind of ore, taking into account the necessity of the material to be subsequently processed by flotation for an efficient separation of the valuable phases.

Figure 1 shows the comminution flowsheet that has been selected in order to test the response of the material to different machines. The aim was to produce material with dimensions smaller than 0.425 mm. Each machine output has been screened at 0.425 mm in order to eliminate the finer part and avoid regrinding of ultrafine particles.

2.3.1 Impact Crusher

A *Hazemag* impact crusher has been used as the first primary crusher. This machine has a four-lug-bolt rotor, powered by an electrical motor. The feeding opening is 120×120 mm.

2.3.2 Jaw Crusher

A *Magutt-10* jaw crusher has been used for the second phase of the primary crushing. It is powered by a 0.75 kW electric engine, at 250 rpm. The selected gap was 5 mm, obtaining a reduction ratio equal to 10.

2.3.3 Disk Mill

A *S.I.M.A. Milano* disk mill has been used as first phase for the secondary crushing. The disk gap selected was 1 mm, obtaining a reduction ratio of 10 at the output.

2.3.4 Rod Mill

A lab-scale rod mill has been used as the final stage of secondary crushing. It is equipped with a 193 mm diameter, 267 mm long drum, containing nine steel rods with a diameter of 8 mm inside, powered by a 0.4 kW electrical engine. The drum has been filled with 1 kg of material at 30% v/v filling ratio. The grinding time has been 4 min.

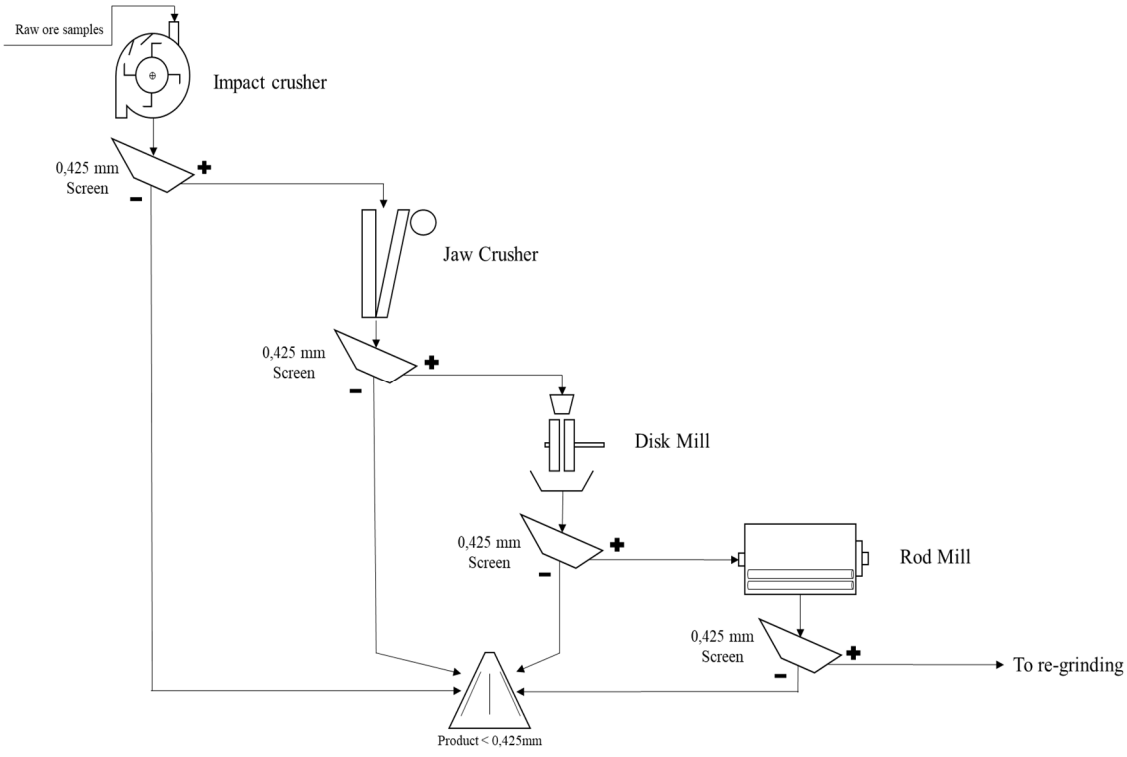

Figure 1. Lab-scale comminution scheme and flowsheet.

2.4 Sieve Snalysis

Sizing of material has been performed using different combinations of sieves in dry and wet conditions, in order to know the size distribution of the comminution output material. Dry sieving has been selected for general output from each crushing and comminution step. A portion of material was collected and screened by means of nested screens in decreasing size from the top screen to 0.125–0.075 mm depending on the fineness of the material and shaken for 3 min in the lab screen shaker.

The purpose of wet sieving was, instead, the understanding of granulometric distribution for all comminution products below 0.425 mm. The sieve sequence consisted of 0.425, 0.355, 0.300, 0.25, 0.212, 0.180, 0.125, 0.090, and 0.063 millimeters, and the screening has been conducted using water as slime-transporting media, especially for ultrafine particle trapping.

3. Results

3.1 Optical Microscopy

Observation of thin sections, shown in Figure 2, has been carried out with OM in parallel transmitted light (PL) and cross-polarized transmitted light (XPL), with objectives between 4× and 10×. There is an abundant presence of sphalerite minerals surrounded by a calcite matrix. Light-opaque mineralization, such as galena and its altered compounds, have been found. It is possible to spot some opaque veins, filled with black organic material.

Sphalerite grains are massively present in the samples, showing a yellow-brownish and black coloration, transparent in PL and opaque in XPL. Calcite appears as a white and striated matrix, transparent both in PL and XPL. Opaque minerals, like galena and cerussite, are sparse and usually occurring in the surroundings of sphalerite grains

Free-grain size, ranging between 0.400 and 0.425 mm, has been defined thanks to digital measurement from OM images.

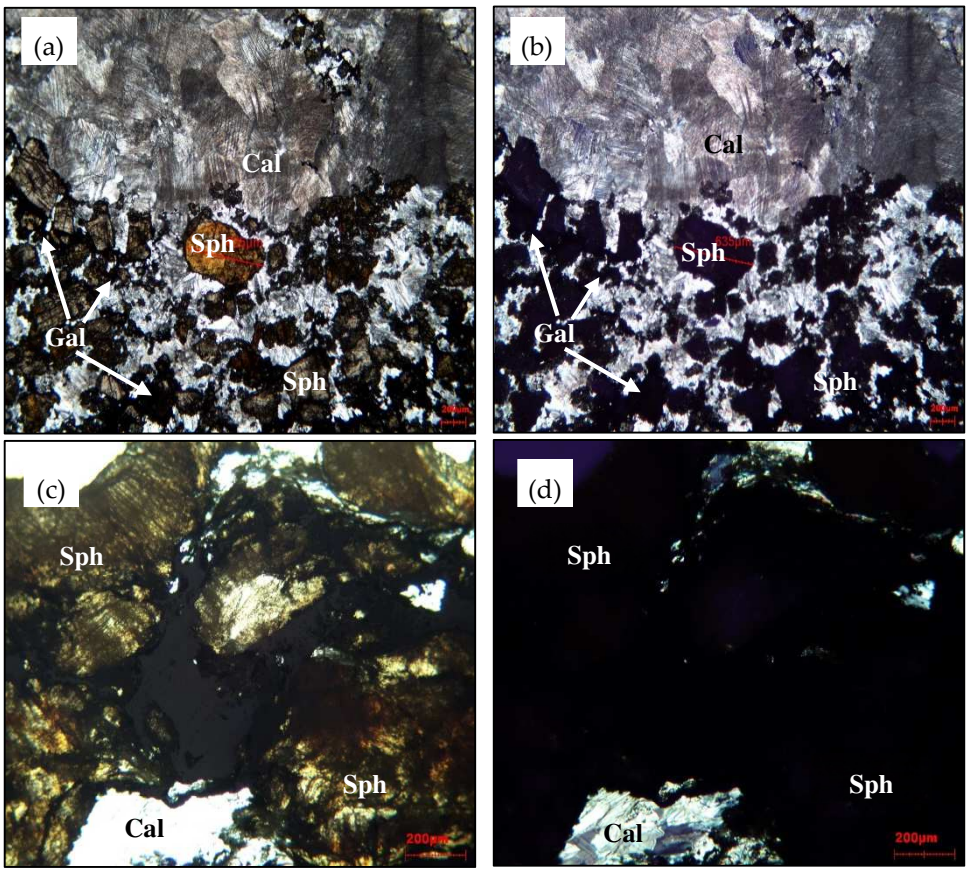

Figure 2. OM thin sections images in PL and XPL (Sphalerite, *Sph*; Calcite, *Cal*; Galena, *Gal*): (**a**) Thin section n.1, PL and (**b**) XPL; (**c**) Thin section n.3, PL and (**d**) XPL.

3.2 Scanning Electron Microscopy

In order to have elemental information related to the mineralization nature, SEM punctual analyses have been performed. The investigation targeted those areas difficult to be characterized by OM and the intergranular filled voids present.

SEM images and EDS spectra, shown in Figure 3, confirmed a widespread presence of sphalerite [24] in the calcite [25] matrix and highlighted the presence of Zn and Pb alteration compounds, mainly cerussite [26], anglesite [27] and smithsonite [28]. The presence of organic matter in the microfractures has been detected [29].

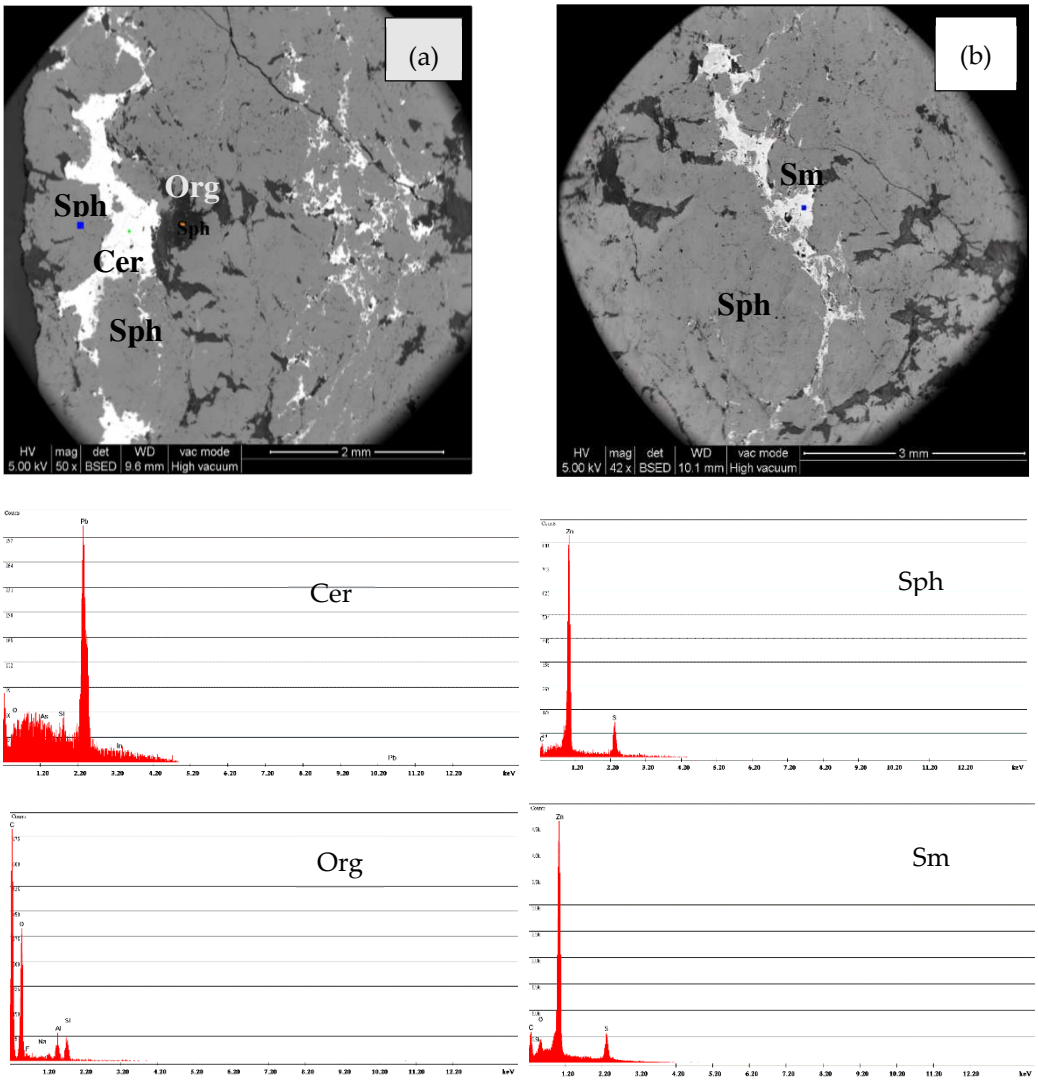

Figure 3. SEM images and spectra of thin sections: (**a**) sphalerite (Sph, blue dot), cerussite (Cer, green dot), organic matter (Org, orange dot); (**b**) sphalerite (Sph) and smithsonite (Sm, blue dot)

3.3 Comminution

The selected flowsheet can be considered as an all-encompassing crushing-comminution process, according to [30,31]. Material enters with maximum size of 250 mm and it is reduced to millimetric and sub-millimetric grains. The purpose of this test was to bring most of the material below the free-grain size, limiting fine and ultrafine fractions that could negatively affect flotation

separation [32,33,34,35]. After a preliminary manual reduction performed with a 5 kg hammer, the process can be divided in two phases [1]:

- primary crushing, with impact crusher and jaw crusher;
- secondary crushing, with disk mill and rod mill.

Each equipment output has been studied for granulometric assessments and reduction ratio checks. Granulometric curves for output material are shown in Figure 4.

As plotted in Figure 5, the impact crusher, selected as the first step of the comminution flowsheet, resulted in a dimension reduction with contained fine production <0.425 mm of 16.2%wt. The jaw crusher, chosen for the second step of primary crushing, gave a lower production of fines. In fact, only 6.9%wt. of <0.425 mm has been obtained. At the end of the primary crushing phase, the overall fraction having dimension below free-grain size is the 22%wt. of the input material, while the overpassing material sent to secondary crushing phases is the 78%wt. In general, primary crushing has been successful in minimizing the fine fraction production and reducing the overall size in a controlled way.

For further size reduction, a disk mill has been selected as the first stage of milling. It resulted in a material characterized by d50 > 1.4 mm, with the fraction of fines being 12.3%wt. The output material is homogeneously sized. A rod mill has been the final step of the circuit. It was selected aiming to a drastic reduction of the material below the free-grain size of 0.425 mm. Results show how 4 min of grinding time produced 56.8%wt. of under-passing material. At the end of secondary crushing tests, material having d < 0.425 mm is 62.1%wt. of the feed material obtained by primary crushing.

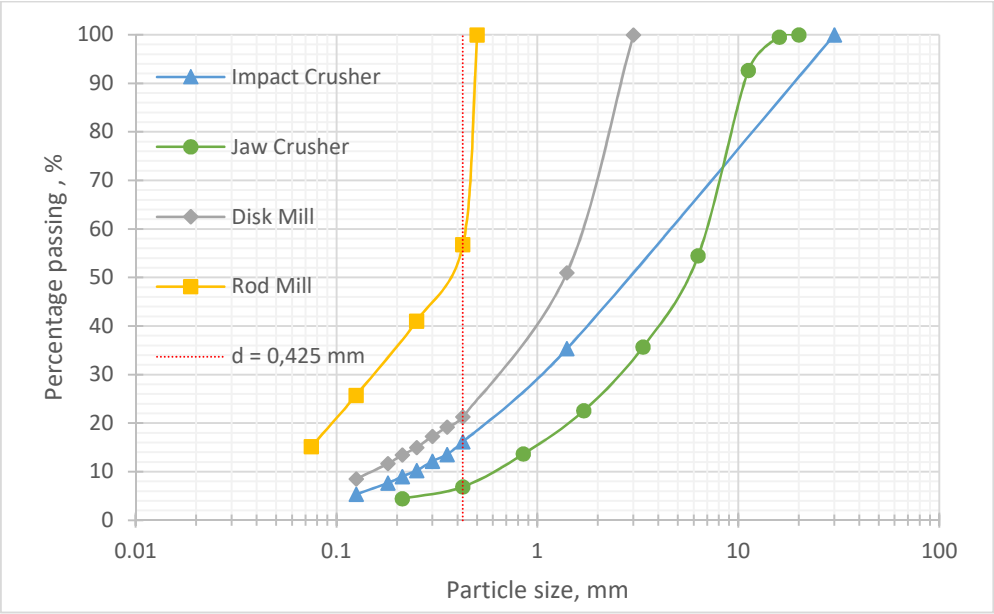

Figure 4. Output product granulometric curves for each equipment.

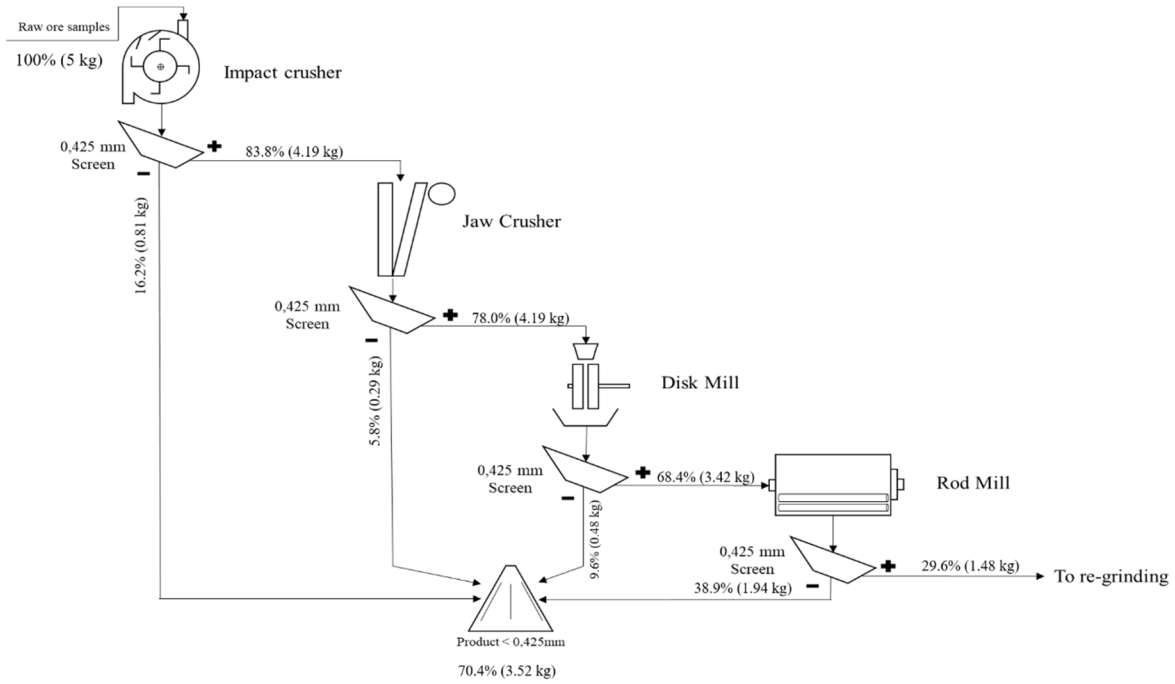

Figure 5. Comminution flowsheet with input and output mass balance.

Reduction ratios of each comminution step have been computed in order to assess the performances of the circuit. The reduction ratio ε is calculated by Eq. 1, with d_{50} being 50% of the cumulative weight of the particle size distribution [36]:

$$\varepsilon = \frac{d_{50,Feed}}{d_{50,Product}}. \quad (1)$$

Figure 6 shows how reduction ratios change among the different equipment considered in the test. A reduction ε = 10 for the impact hammer follows a relevant reduction in dimension of material, as usual for primary crushing [31]. The jaw crusher outputs' reduction ratio drops to ε = 1.8 due to a very low production of fines. For the milling phase, the disk mill and rod mill show slightly increasing ε values of 3.1 and 3.7, respectively. Overall, the reduction ratios show that the most impacting step on the size decrease of the material is primary crushing. Secondary crushing is characterized by ε smaller than common practice comminution performances [31].

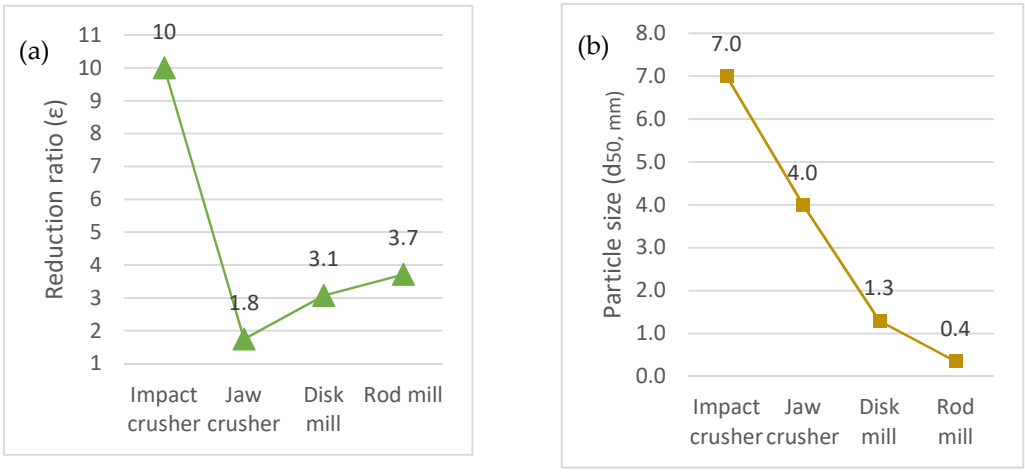

Figure 6. Performance parameter for comminution and product dimensions: (**a**) Reduction ratio trend related to equipment; (**b**) Change of d_{50} among comminution products

Overpassing material, accounting for about 30%, has not been reintroduced in any grinding stage, as the overall flowsheet has been arranged as an open-like comminution circuit [1]. All under-passing materials have been collected together and further analyzed as ground product.

3.4 Product Sizing

Comminution products passing the 0.425 mm threshold have been more specifically analyzed in terms of granulometric distribution in order to better understand the presence of fine and ultrafine particles. This has been necessary for the assessment of the comminution behavior of the ore, aiming to deliver a good quality material for further separation steps.

Wet sieving methodology has been selected. In Table 1, mesh size and retained and passing material is shown.

Table 1. Retained fractions and passing percentage resulting from wet sieving.

Mesh size (mm)	Retained weight fraction (%)	Percentage passing (%)
0.425	0	100
0.350	13.8	86.2
0.300	6.9	79.3
0.250	8.8	70.5
0.212	6.2	64.3
0.180	6.4	57.9
0.125	13.5	44.4
0.090	8.4	36.0
0.063	8.8	27.2
−0.063	27.2	---

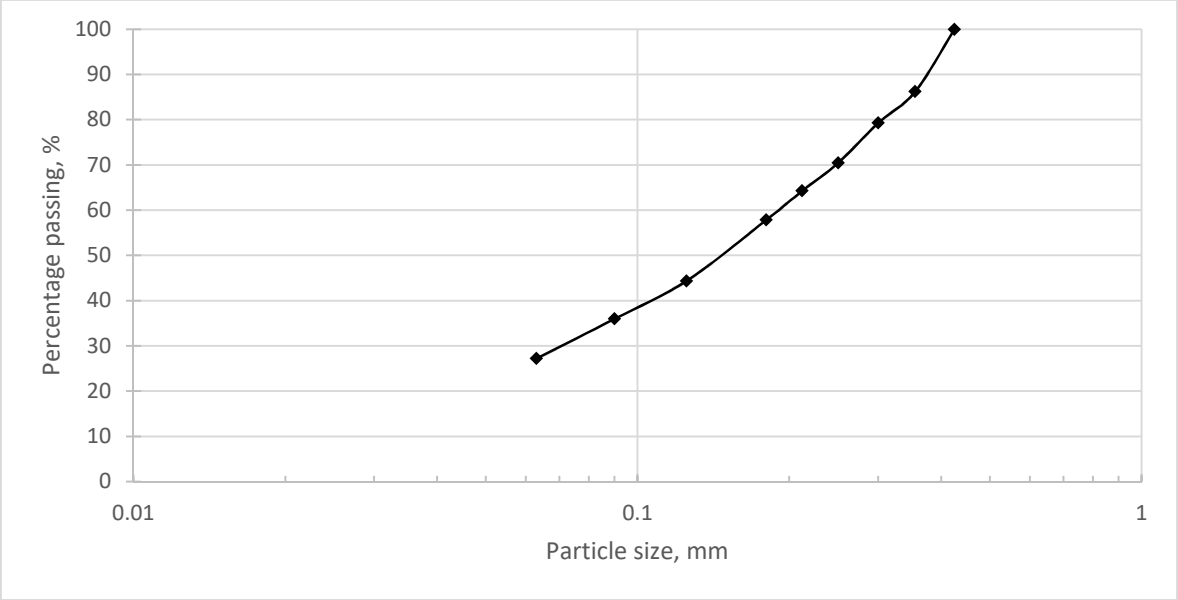

Figure 7. Granulometric curve obtained by means of wet sieving on comminution products <0.425 mm

Figure 7 shows the granulometric curve which has been obtained from previous data, resulting in values of d_{80} = 0.300 mm and d_{50} = 0.160 mm. These findings show that the presence of very fine fractions is relevant. In fact, material below 0.063 mm is 27.2%wt. of the total considered sample. This behavior can be explained by the natural texture of the ore and the mechanical properties of the minerals contained.

3.5 X-Ray Powder Diffraction Analyses

XRPD analyses, performed on each dimension class obtained by wet sieving, distinguished five different mineral phases: sphalerite, galena, calcite, anglesite, and cerussite as reported in Figure 7. Sphalerite's main peaks has been observed at 2θ angles of 28,57°, 33.11°, 47.57°, 56.39°, 76.77° and 88.52° [37]. Calcite's representative peaks have been observed at 2θ angles of 29.44° and 48.58° [38]. Galena's peaks have been observed at 2θ angles of 26°, 30.09°, 43.06°, and 50.98° [39]. Cerussite's and Anglesite's characteristic peaks have been observed at 2θ angles of 24.80°, 25.49°, 43,48° and 20.84°, 23.36°, 26.75° respectively [40,41].

Qualitatively, each class showed a constant presence in terms of mineral phases. Reference spectra [37-41, 23] have been compared with the experimental ones. These outcomes generally confirmed what was previously observed by OM and SEM.

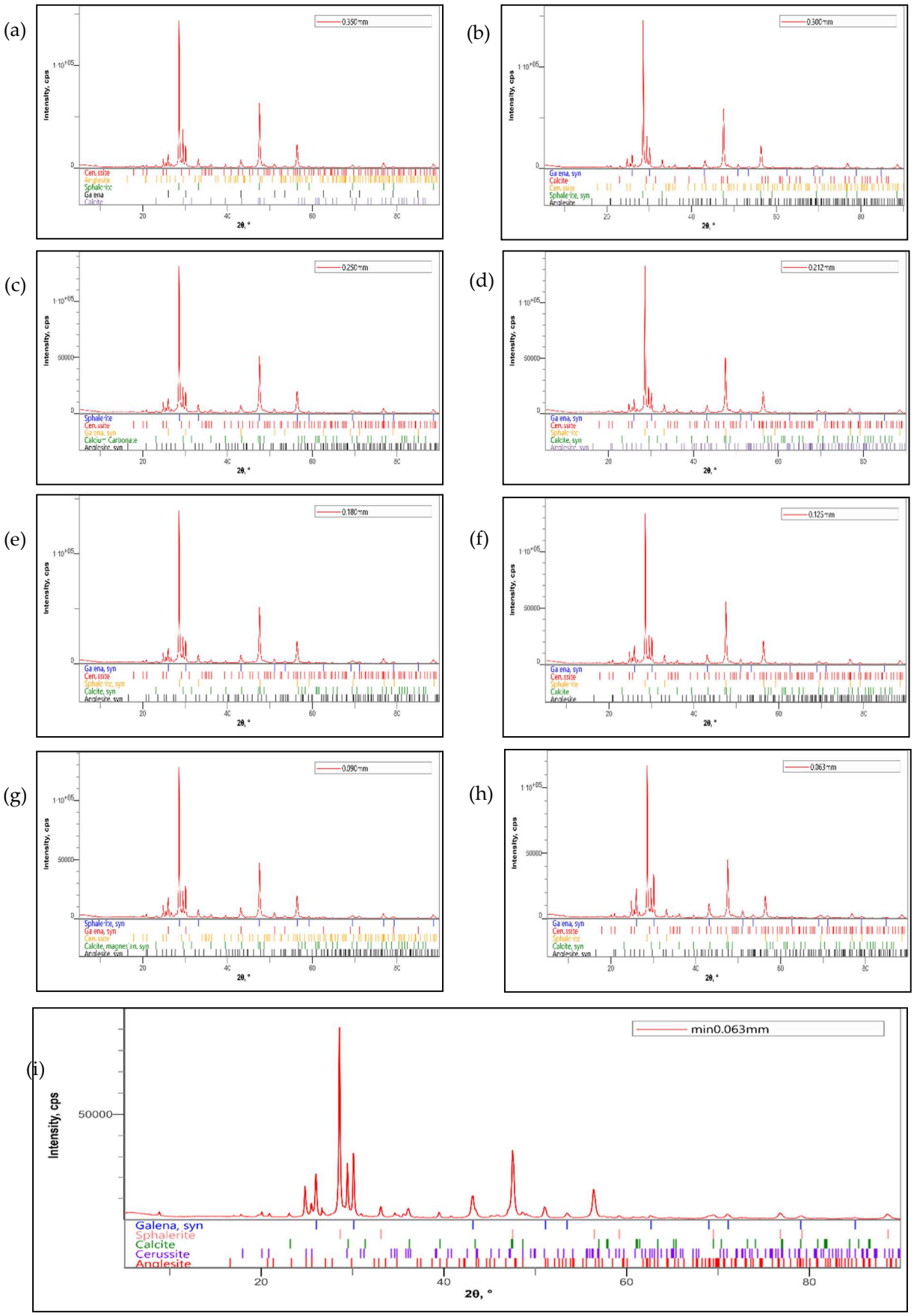

Figure 8. XRPD spectra of comminution product sieved classes: (a) 0.425–0.350 mm, (b) 0.350–0.300 mm, (c) 0.300–0.250 mm, (d) 0.250–0.212 mm, (e) 0.212–0.180 mm, (f) 0.180–0.125 mm, (g) 0.125–0.090 mm, (h) 0.090–0.063 mm, (i) <0.063 mm.

Quantitative XRPD analyses obtained by Rietveld [20-22] refinement showed residual errors R_{wp} ranging from 5.50% to 6.49% and goodness-of-fit in the range from 2.06 and 2.41 as shown in Table 2.

Table 2. Observed residual errors (R_{wp}) and goodness-of-fit (S) from quantitative XRPD analysis.

Particle size (mm)	R_{wp} (%)	S
0.425–0.350	5.90	2.20
0.350–0.300	5.54	2.07
0.300–0.250	5.55	2.07
0.250–0.212	5.55	2.06
0.212–0.180	6.21	2.33
0.180–0.125	5.50	2.05
0.125–0.090	5.86	2.20
0.090–0.063	5.87	2.21
<0.063	6.49	2.41

According to some authors, a Rietveld refinement showing low R_{wp} and S values can be considered as reliable with errors in weight fraction estimation between 0.5%wt. and 1.5%wt. [42,43]. Quantitative results are shown in Table 3. On average, sphalerite is the most abundant phase in the samples, ranging 50–70%wt., calcite defined as gangue mineral attained 17–27%wt., while galena ranges 4–9%wt. Other phases can be considered as minor. The accuracy of the quantitative analyses has not been assessed in detail.

Table 3. Quantitative XRPD results for each particle size.

Particle size class (mm)	Weight Fraction (%)[1]				
	ZnS	PbS	$PbCO_3$	$PbSO_4$	$CaCO_3$
0.425–0.350	65.59	4.09	2.52	2.93	24.87
0.350–0.300	66.82	4.14	3.04	2.67	23.33
0.300–0.250	69.32	4.28	3.08/	2.50	20.82
0.250–0.212	67.35	4.12	3.11	3.55	21.87
0.212–0.180	70.39	4.60	3.71	4.04	17.26
0.180–0.125	68.22	5.37	3.27	2.79	20.35
0.125–0.090	65.88	6.54	3.97	4.10	19.51
0.090–0.063	62.63	8.41	4.94	3.53	20.49
<0.063	51.50	7.97	6.43	7.20	26.90

1. Estimation errors must be considered in the range ± 0.5–1.5% according to [42,43]

Some of the mineral phases present in the samples show a different concentration among different granulometric classes. The clearest evidence is the one linked with galena and Pb-related compounds. Their total concentration is around 9.5%wt. in particle size 0.425–0.350 mm and reaches 21.6%wt. in particle size <0.063 mm, constantly increasing their presence with the decrease of material dimension. Galena is the most abundant regarding Pb-related compounds and shows a worthwhile concentration for further recovery.

Sphalerite is the most abundant phase in each size, but its presence decreases from 0.180 mm, where it peaks with 70.4%wt., toward finer classes. The lowest concentration of ZnS is 62.6%wt., found in the <0.063 mm class. The calcite phase has its lowest presence in class 0.212–0.180 mm with 17.3%wt., while its highest concentration of 26.9%wt. is measured in the <0.063 mm class.

In general, high values of valuable minerals have been found in the different classes of comminution products, underling the necessity of further separation in order to obtain high quality concentrates from the ore. In the choice of recovery and separation methods of Pb-related minerals,

249 galena in particular, the increase of their concentration in the finest classes should be taken in
250 consideration.

251 **4. Discussion**

252 The purpose of this study was to understand the distribution of target minerals among mineral
253 processing products, particularly after a lab-scale comminution test. In order to have an overview of
254 the characteristics of the sampled ore, petrographic observations have been necessary for the
255 determination of the shape, composition and dimension of grains present in the mineralized mixed
256 sulfide ore collected in an MVT deposit in Northern Italy. As described above, thin sections have
257 been realized and observed. Results showed typical characteristics related to MVT deposits [19,44],
258 with relatively high content of sphalerite minerals embedded in a calcite matrix. Galena is sparsely
259 present in very small crystals, difficult to be distinguished only by OM.
260 SEM characterization brought additional information, especially concerning alteration products
261 and filling of the ore's microfractures. The presence of cerussite, anglesite and organic matter has
262 been detected, confirming the presence of Pb-related minerals and traces of organic matter, arguably
263 linked with the formational geological environment of the site [19]. The observation made on the
264 dimensional characteristics resulted in an estimated liberation size of valuable minerals ranging
265 between 0.400 and 0.450 mm. On these parameters, a lab-scale comminution open circuit has been
266 arranged, with the rod mill being the phase that mostly controls the final output products. A 30%wt.
267 of the initial input material needs to be reground and has not been considered (Figure 5). Ground
268 product contains 27%wt. of material <0.063 mm (Table 1).
269 XRPD quantitative analyses highlighted the important presence of sphalerite and galena in
270 dimension classes ranging between the 0.250 and 0.063 mm classes, as shown in Figure 8a and Figure
271 8d. This size range is considered suitable for separation processes such as froth flotation or
272 gravimetric methods [1,45,46]. Concerning the presence of Pb-related compounds in very fine classes,
273 a non-conventional flotation [47,48] should be tested. Target phase concentration has been observed
274 as fluctuating, varying with the reduction in dimension of products (Figure 9). This phenomenon
275 could be framed in a selective comminution behavior of the ore [36], but in this study further data
276 should be collected in order to better define parameters related to this specific possibility.

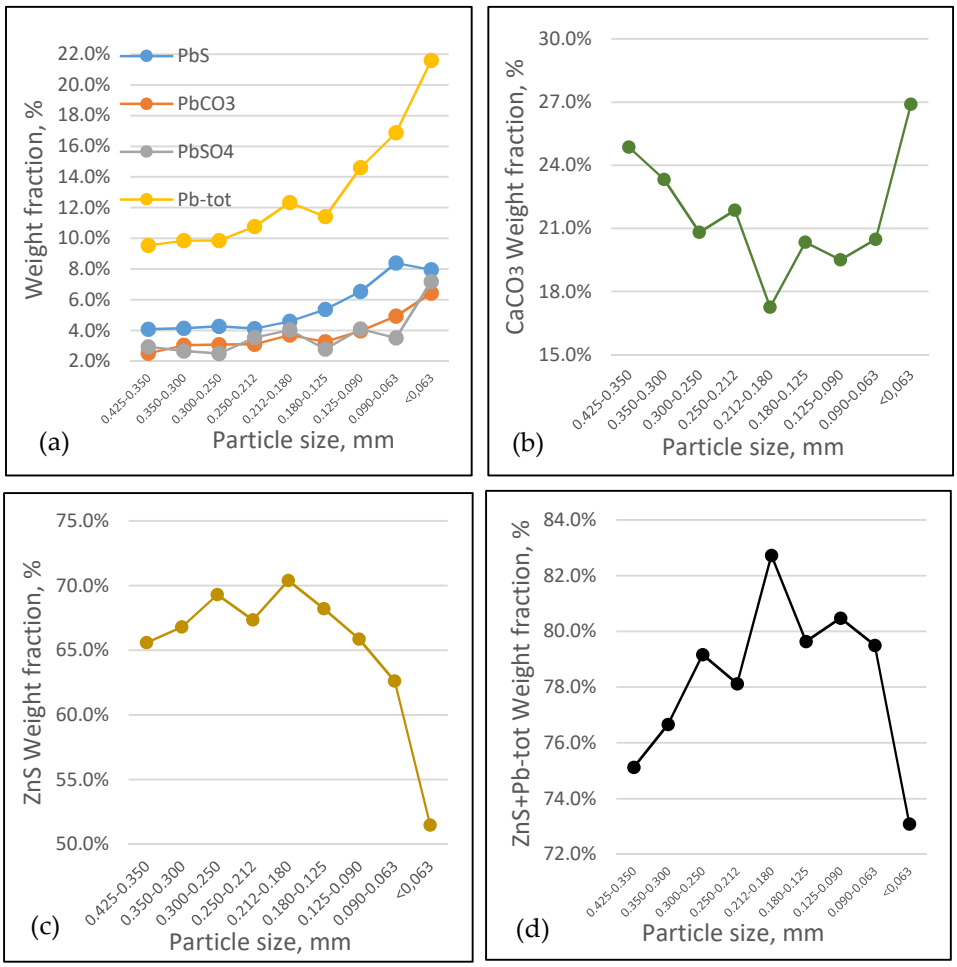

Figure 9. Mineral phases weight fraction variation among dimension classes in comminution products below 0.425 mm: (**a**) Pb-related compounds, (**b**) calcite, (**c**) sphalerite, (**d**) valuable phases assumed as sum of sphalerite and Pb-related compounds.

The calcite trend appears as V-shaped, encountering a descending behavior until the 0.212–0.180 mm class, strictly related to total valuable phase ZnS + Pb-tot peak.

Considering the sum of ZnS and Pb-related, plotted in Figure 9d and corresponding to the valuable minerals present in the ore, their trend is mainly dominated by sphalerite oscillations in the samples (Figure 9c). Peak concentration is reached in the 0.212–0.180 mm class with 82.7%wt., while their lowest occurrence of 73.1%wt. is in the <0.063 mm particle size, as shown in Figure 9d.

Moreover, thanks to quantitative analyses, important information has been obtained for the evaluation of the most suitable dimension classes to be delivered to following separation stages. This important trend should be considered for further studies related to the mineral recovery rate achievable by froth flotation. Generally, the amount of valuable mineral phases is relevant and worthwhile. Further detailed studies should be taken into consideration.

Acknowledgments: Authors are thankful to Alta Zinc Ltd and Energia Minerals (Italia) S.r.l. for the availability in welcoming access, interest, recovery and sharing of relevant information related to their industrial activities.

Author Contributions: Conceptualization, G.B. and P.M.; Methodology, G.B. and P.M.; Investigation, G.B. and O.B.; Resources, P.M.; Data Curation, G.B.; Writing—Original Draft Preparation, G.B.; Writing—Review and Editing, G.B., O.B. and P.M.; Supervision, P.M.

Conflicts of Interest: The authors declare no conflict of interest.

References

1. Wills, B.A. Comminution in the minerals industry — An overview. *Miner. Eng.* **1990**, *3*, 3–5.
2. Ozgur O.; Hakan B. Comparison of different breakage mechanisms in terms of product particle size distribution and mineral liberation. *Miner Eng.* **2013**, *49*, 103–108
3. Hoşten Ç.; Özbay C. A comparison of particle bed breakage and rod mill grinding with regard to mineral liberation and particle shape effects. *Miner. Eng.* **1998**, *11*, 871–874.
4. King R.P. Comminution and liberation of minerals. *Miner. Eng.* **1994**, *7*, 129–140.
5. Nadolski S.; Bern K.; Amit Z.; Zorigtkhuu D. An energy benchmarking model for mineral comminution. *Miner. Eng.* **2014**, *65*, 178–186.
6. Tromans D. Mineral comminution: Energy efficiency considerations. *Miner. Eng*. **2008**, *21*, 613–620.
7. Mwanga A.; Rosenkranz J.; Lamberg P. Testing of ore comminution behavior in the geometallurgical context – A review. *Minerals* **2015**, *5*, 276–297.
8. King R.P. *Modeling and Simulation of Mineral Processing System*. Elsevier, 2001; pp. 127–212.
9. Bazin C.; Grant R.; Cooper M.; Tessier R. A method to predict metallurgical performances as a function of fineness of grind. *Miner. Eng.* **1994**, *7*, 1243–1251.
10. Pérez-García E.M; Bouchard J.; Poulin É. Simulation analysis of a mineral liberation estimator for control purposes. *IFAC-Pap*. **2019**, *52*(14), 123–128.
11. Pérez-García E.M; Bouchard J.; Poulin É. Integration of a liberation model in a simulation framework from comminution circuits. *Miner. Eng.* **2018**, *126*, 167–176.
12. Palm N.A.; Shackleton N.J.; Malysiak V.; O'Connor C.T. The effect of using different comminution procedures on the flotation of sphalerite. *Miner Eng.* **2010**, *23*, 1053–1057.
13. Wei Y.; Sandenbergh R.F. Effects of grinding environment on the flotation of Rosh Pinah complex Pb/Zn ore. *Miner. Eng.* **2007**, *20*, 264–272.
14. Mudenda C.; Mwanza B.G.; Kondwani M. Analysis of the effects of grind size on production of copper concentrate: A case study of mining company in Zambia. *International Conference on Chemical Processes and Green Energy Engineering (ICCPGEE'15), July 14–15, 2015, Harare, Zimbabwe*; 2015.
15. Liu L.; Tan Q.; Liu L.; Cao J. Comparison of different comminution flowsheets in terms of minerals liberation and separation properties. *Miner. Eng.* **2018**, *125*, 26–33.
16. Wei Y.; Sandenbergh R.F. Effects of grinding environment on the flotation of Rosh Pinah complex Pb/Zn ore. *Miner. Eng.* **2007**, *20*, 264–272.
17. Forssberg E.; Sundberg S.; Zhai H. Influence of different grinding methods on floatability. *Int. J. Miner. Process.* **1988**, *22*, 183–192.
18. Wang X.H.; Xie Y. The effect of grinding media and environment on the surface properties and flotation behaviour of sulphide minerals. *Miner. Proc. Extr. Met. Rev.* **1990**, *7*, 49–79.
19. Mondillo N.; Lupone F.; Boni M.; Joachimski M.; Balassone G.; De Angelis M.; Zanin S.; Granitzio F. From Alpine-type sulfides to nonsulfides in the Gorno Zn project (Bergamo, Italy). *Miner. Deposita* **2019**, *55*, 953–970.
20. Rietveld H. A profile refinement method for nuclear and magnetic structures. *J. Appl. Cryst.* **1969,** *2*, 65–71.
21. Young R.A. *The Rietveld Method*. **1993**, International Union of Crystallography, Oxford University Press.
22. McCusker L.B.; Von Dreele R.B.; Cox D.E.; Louer D.; Scardi P. Rietveld refinement guidelines. *J. Appl. Cryst.* **1986**, 32, 36-50.
23. ICDD. PDF-4/Minerals; International Centre for Diffraction Data: Newtown Square, PA, 2020.
24. Mineralogy Database. http://webmineral.com/data/Sphalerite.shtml.
25. Mineralogy Database. http://webmineral.com/data/Calcite.shtml.
26. Mineralogy Database. http://webmineral.com/data/Cerussite.shtml.
27. Mineralogy Database. http://webmineral.com/data/Anglesite.shtml.
28. Mineralogy Database. http://webmineral.com/data/Smithsonite.shtml.
29. Ohkouchi N.; Kuroda J.; Taira A. The origin of Cretaceous black shales: A change in the surface ocean ecosystem and its triggers. *Proc. Japan Acad. Ser. B. Phys. Biol. Sci.* **2015**, *91*(7), 273–291.
30. Mwanga A.; Lamberg P.; Rosenkranz R. Comminution test method using small drill core samples. *Miner. Eng.* **2015**, *72*, 129–139.
31. Gupta A.; Yan D. S. *Mineral processing design and operation: An introduction*; Elsevier, 2006; pp. 123–152.
32. Pérez-Garibaya R.; Ramírez-Aguileraa N.; Bouchardb J.; Rubio J. Froth flotation of sphalerite: Collector concentration, gas dispersion and particle size effects. *Miner. Eng.* **2017**, *57*, 72–78.

33. Duarte A.C.P.; Grano S.R. Mechanism for the recovery of silicate gangue minerals in the flotation of ultrafine sphalerite. *Miner. Eng.* **2007**, *20*(8), 766–775.
34. Collins G. L.; Jameson G. L. Experiments on the flotation of fine particles, the influence of particle size and charge. *Chem. Eng. Sci.* **1976**, *31*, 985–991.
35. Arbiter N. Problems in sulfide ore processing. *Beneficiation of Mineral Fines — Problems and Research Needs*; P. Somasundaran; N. Arbiter, Eds.; AIME: Ann Arbor, MI, 1979, pp. 139–152.
36. Hesse M.; Popov O.; Lieberwirth H. Increasing efficiency by selective comminution. *Miner. Eng.* **2017**, *103–104*, 112–126.
37. RRUFF. https://rruff.info/R040136.
38. RRUFF. https://rruff.info/R040070.
39. RRUFF. https://rruff.info/R070325.
40. RRUFF. https://rruff.info/R040069.
41. RRUFF. https://rruff.info/R040004.
42. Monecke T.; Köhler S.; Kleeberg R.; Herzig P.M.; Gemell J.B. Quantitative phase-analysis by the Rietveld method using X-ray powder-diffraction data: Application to the study of alteration halos associated with volcanic-rock-hosted massive sulfide deposits. *Canad. Mineral.* **2001**, *39*, 1617–1633
43. Zhao P.; Lu L.; Liu X.; De la Torre A.G.; Cheng X. Error analysis and correction for quantitative phase analysis based on Rietveld-internal standard method: Whether the minor phases can be ignored? *Crystals* **2018**, *8*(3), 110.
44. Paradis S.; Hannigan P.; Dewing K. Mississippi Valley-type lead-zinc deposits (MVT). *Mineral Deposits of Canada*; Geological Association of Canada, 2007, pp. 185–203.
45. Trahar W. J.; Warren L. J. The floatability of very fine particles-a review. *Int. J. Miner. Process.* **1976**, *3*, 103–131
46. Gaudin A. M.; Groh J. O.; Henderson H. B. Effect of particle size on flotation. *AIME Tech. Pub.* **1931**, *414*, 3–23.
47. Song S.; Lopez-Valdivieso A.; Reyes-Bahena J.L.; Lara-Valenzuela C. Floc Flotation of galena and sphalerite fines. *Miner. Eng.* **2001**, *14*, 87–98.
48. Song S.; Lopez-Valdivieso A.; Reyes-Bahena J.L.; Bermejo-Perez H.I; Trass O. (2000). Hydrophobic flocculation of galena fines in aqueous suspensions. *J. Colloid Interface Sci.* **2000**, *227*, 272–281.